SCIENCE CHINA
Earth Sciences

•RESEARCH PAPER•

April 2023 Vol.66 No.4: 871–881
https://doi.org/10.1007/s11430-022-1035-4

Multi-site observation of large-scale eddies in the surface layer of the Loess Plateau

Jinbei CHEN[1,2*], Xiaowen CHEN[3], Wei JIA[1], Ye YU[1] & Suping ZHAO[1]

[1] *Key Laboratory of Land Surface Process and Climate Change in Cold and Arid Regions; Northwest Institute of Eco-Environment and Resources, Chinese Academy of Sciences, Lanzhou 730000, China;*
[2] *Key Laboratory of Middle Atmosphere and Global Environment Observation (LAGEO), Institute of Atmospheric Physics, Chinese Academy of Sciences, Beijing 100029, China;*
[3] *Mechanical Engineering Department, Pennsylvania State University, State College 16802, USA*

Received July 6, 2022; revised November 5, 2022; accepted November 22, 2022; published online March 16, 2023

Abstract This article aims to build a theory of atmospheric boundary layer turbulence under complex conditions. To achieve this goal, we constructed a multi-site observation and analysis method of atmospheric turbulence based on related principles. This method first requires verification for the ergodicity of the full-scale observation of surface-layer turbulence, which proves that eddies within a scale of 60 min during a four-site observation can easily meet ergodicity. Meanwhile, by applying the second-order structure function for the horizontal wind speed turbulence of a single site and upstream and downstream points, we verified the ergodicity of the turbulence observation. Comparing the turbulence spectrum to the second-order structure function for the horizontal wind speed from the four-site observation, a relatively high accordance was observed, proving the reasonability of the multi-site observation. Moreover, compared to the single-site observation, the four-site observation can improve the estimation accuracy of the surface-layer turbulence spectrum and vertical turbulent flux. As a result, we can describe the three-dimensional structure of turbulence more accurately and comprehensively by combining analytical data from single-site and four-site observations. In summary, the multi-site turbulence observation method shows that the horizontal and vertical wind turbulence of the Baimiao plateau has a typical structure of a turbulence spectrum with clear spectral gaps. The result is in accordance with the scale of the turbulence spectral gaps obtained from the 6 h data. The horizontal wind speed is under the influence of the terrain, so its spectrum of large-scale eddies has higher fluctuations, but its spectral gaps can still be clearly distinguished. Although the spectral gaps of the temperature spectrum are not distinguishable, they still have the same scale as the spectral gap of the vertical and horizontal turbulence spectrum. Moreover, the temperature spectrum possesses typical structure characteristics of the boundary-layer turbulence spectrum.

Keywords Larger-scale eddy, Complex condition, Ergodicity of turbulence observation, Structure function, Turbulence spectrum

Citation: Chen J, Chen X, Jia W, Yu Y, Zhao S. 2023. Multi-site observation of large-scale eddies in the surface layer of the Loess Plateau. Science China Earth Sciences, 66(4): 871–881, https://doi.org/10.1007/s11430-022-1035-4

1. Introduction

The theories of energy cascade and isotropic isotropy introduced by Richardson (1922), Taylor (1935a, 1935b, 1935c, 1935d), and Kolmogorov (1941, 1962) are the foundation of research of turbulence in various fields. However, isotropic turbulence is merely an approximation of small-scale turbulence that is far from the boundary and has a high Reynolds number. However, in reality, turbulence is always under the influence of the geometric boundary condition instead of the forced influence of "rotational invariance," required by isotropy (Hunt and Carlotti, 2001;

* Corresponding author (email: chenjinbei@lzb.ac.cn)

Biferale and Procaccia, 2005). The effect of energy transfer and stress force among eddies with various scales on the formation and evolution of turbulence structures is still one of the most concerning problems in turbulence research. In the past 20 years, many important advances have already been made in turbulence eddies and the mechanisms of anisotropy formations (Hunt and Carlotti, 2001; Biferale and Procaccia, 2005; Pavidson, 2004; Zhang et al., 2012). The findings have already shown that, at the beginning of turbulence, the effect of the dynamic shear is top-down, while the effect of the thermodynamic gradient is bottom-up (Hu et al., 2007). Under these shear effects, tubular, linear, or even flake eddies appear in the flow field. Meanwhile, under the effect of flow field shearing, these vortices, being stretched and squeezed, increase their vorticity and form turbulent eddies. The atmospheric-boundary-layer turbulence is a typical system that forms under the effects of ground-surface heating power and dynamic shearing, and this system has a relatively complete process of energy input and dissipation (Hu et al., 2007). Under the effects of the weather system and ground-surface thermodynamics and based on the energy transfer characteristics of the spectrum of atmospheric-boundary-layer turbulence, three eddy structures can be identified from the surface-layer turbulence: (1) Large-scale eddies (very-large-scale motion). They can gain energy from fluid shear with a large scale, and their energy spectrum satisfies $kS_u \sim k^{+1}$, which corresponds to the boundary-layer scale δ and $k<1/\delta$ (k is the wave number $k=1/\lambda$ and S_u is the density of the energy spectrum). (2) Attached eddies, with energy spectra of $1/\delta<k<1/z$ (z is the height above the ground). Turbulence coherent structures typically form in this scale range. (3) Detached eddies. These turbulences are often isotropic. In the range of $1/z<k<1/\eta$, where $\eta=(\nu^3/\varepsilon)^{1/4}$ (ν is the air viscosity and ε is the dissipation rate of the turbulent kinetic energy), the turbulences satisfy $kS_u \sim k^{-2/3}$. When the observation point is close to the ground surface, under the influence of a strong shearing, separation vortices will not satisfy isotropy, and the attenuation rate of the energy spectrum will also slightly deviate from −2/3 (Drobinski et al., 2004). However, such a deviation does not change the essence of the energy cascade of detached eddies. Meanwhile, large-scale eddies and attached eddies have a relatively large difference due to the change in the thermal and dynamic conditions at the boundary. When large-scale eddies are close to the ground surface, they can be deformed due to the stretching and squeezing caused by boundary shearing, and they can be further torn into eddies with a low-scale level (Hunt and Carlotti, 2001). The process of gaining and transporting energy by these large-scale eddies controls the structure of the turbulences and the turbulent transport of matter and energy. Obviously, these large-scale eddies are the dominator of boundary-layer turbulence systems. Therefore, the accurate measurements of large-scale eddy intensities and structures and the study of the energy gain and transportation process are crucial issues in boundary-layer turbulence research.

The turbulence structures of large-scale, attached, and detached eddies correspond to space scales with a range of 10^{-5}–10^{2} km (Stull, 1988; Ghannam et al., 2018). Starting from the early 20th century, surface-layer turbulence research and energy spectrum analysis are mostly based on single-site observations. Nowadays, people have got a deeper understanding of the space scale and complex systematic structure of surface-layer turbulences, and sensors related to turbulent eddy covariance have become more advanced. Therefore, many researchers have started to use multi-site observation and various remote sensing instruments for large-area observations to improve observation accuracy (Poulos et al., 2002; Oncley et al., 2002; Liu et al., 2016). However, because the calibrations of remote sensing instruments are also based on the eddy-covariance method, a theory needs to be built to improve the eddy-covariance multi-site observations.

Based on the statistical theory of turbulence, the turbulence spectrum is determined by a long-time series in single-site observation data under an assumed ergodicity condition (Stull, 1988). Moreover, the observation can satisfy ergodicity for the single-site turbulence observation of eddies with a scale within 10 min (Chen et al., 2015, 2021). Theoretically, the requirement of an ensemble average can be satisfied by increasing observation sites and capturing the data of attached eddies and large-scale eddies thoroughly when observing the three-dimensional spatial structure of large-scale turbulence. Meanwhile, making large-scale eddies satisfying ergodicity can further improve the accuracies of large-scale eddies and turbulence spectrum. A rather stricter requirement of satisfying ergodicity is required for turbulence observations to guarantee the accuracy of experiments, especially under complex conditions. Moreover, the second-order structure function of the turbulence wind velocity is the secondary moment of difference in the space distance $r\hat{e}_x$ of the wind velocity u_i (the subscripts i, j, and z, which will be brought up later, represent the three directions of the Cartesian coordinate system). Meanwhile, the second-order structure function corresponds to the turbulence spectrum (Kolmogorov, 1941, 1962; Lindborg, 1999; Ghannam et al., 2018). The assumptions of ergodicity usually used in experiments determine the second-order structure functions from single-site observations by relating the dimensions of time and space together. Therefore, a comparison of the second-order structure function between two-site and single-site observations provides a more reasonable verification method than the Monin–Obukhov (M–O) similarity theory (Chen et al., 2015). On the contrary, after the second-order structure function is verified, the turbulence observation satisfying the ergodicity can ensure the accuracy of the tur-

bulence estimation. In summary, we will use multi-site observations to comprehensively and accurately study the structure and spatiotemporal distribution characteristics of turbulent large-scale eddies on complex conditions by combining the turbulence spectrum and turbulence second-order structure function.

The "tableland" of the Loess Plateau is a platform at the top of a mountain, surrounded by deep gullies and ravines. Large-scale eddies tend to exist for a long time on this unique terrain (Chen et al., 2021). Accordingly, this study first established a processing method for multi-site observation data and then analyzed the ergodicity of large-scale eddy data derived from the four-site turbulence observation in a typical tableland. The second-order structure function determined by the single-site and two-site data was used to verify the applicability of the ergodicity function of the turbulence observation. Then, the rationality of the processing method of multi-site data was verified by comparing the corresponding relations between the turbulence spectrum and second-order structure function determined by single-site and four-site data. At the same time, the Ogive function (Oncley et al., 1996; Zuo et al., 2012) was applied to discuss the necessity of determining the turbulent flux through a multi-site observation. Finally, the applicability of the four-site data processing method was discussed. This study aims to develop an observation and analysis method of turbulent structures and fluxes in the surface layer under complex conditions based on the Reynolds mean principle without considering the horizontal uniformity and steady-state conditions.

2. Theoretical background

2.1 Multi-site observation of the turbulence spectrum

The ensemble average of turbulence statistics is defined as the mean of a quantity that is a function of the micro-state of the whole turbulence field. However, in early turbulence observation studies, due to the lack of instruments, the ensemble average is mostly replaced by a single-site long-term average under the assumption of ergodicity (Stull, 1988; Foken et al., 2004). Moreover, if the observation time is prolonged to ensure the ergodicity of large-scale eddy observations, the turbulence field will be unsteady, violating the observation requirements of the classical atmospheric-boundary-layer turbulence theory. For a comprehensive observation of the large-scale turbulence structure, ideal ergodicity needs to be met. Moreover, ergodicity can only be achieved using a suitable spatial–multi-site observation for the conversion between the dimensions of time and space. Multi-site observations satisfy not only the requirements of the steadiness of the turbulence field but also the theoretical requirements of the ensemble average of the observation results (Chen et al., 2015).

Taking the horizontal flow field as an example, under ergodicity conditions, any stationary random variable observed at a single point satisfies $A(x, y, t)=A(x, y, t+\tau)$ (τ is the relaxation time), and any stationary random variable observed at two points on the streamline satisfies $A(x, y, t)=A(x+l_x, y+l_y, t)$, where $l_x=u\tau$, $l_y=v\tau$. The variable from the two-site observation in the space dimension can be transformed into another variable from the single-site observation in the time dimension, that is, $A(x, y, t+\tau)=A(x+l_x, y+l_y\, t)$, and vice versa. Similarly, the multi-site observation of stationary random turbulence does not change the dimension of variable A, but the observation is consistent with the principle of ensemble averaging. The key problem is to transform the spatiotemporal series of multiple-site observation into the temporal series so that the turbulence spectrum can be accurately estimated by Fourier variation. A simple method is to connect the time series of observation data from every single site end to end. Then the distance between observation points (l_x, l_y) and the horizontal wind velocity determine the spatiotemporal relationship of the observation results $A(x, y, t+\tau_e) = A(x+l_x, y+l_y, t)$. That is, the time series $A(j)$ and $A(m)$ at two observation points are used to construct a new series $A(j\ldots m)$. Essentially, the new series may change the mean value μ_A and autocorrelation function $R_A(\tau)$ of turbulence to (Chen et al., 2015, 2021).

$$\mu_A = \lim_{T\to+\infty}\frac{1}{T}\left[\int_0^{T_1}A(t)\mathrm{d}t+\int_{T_1}^{T_2}A(t)\mathrm{d}t\right] = E[A(t)], \tag{1}$$

$$R_A(\tau) = \lim_{T\to+\infty}\frac{1}{T}\left[\int_0^{T_1}A(t)A(t+\tau)\mathrm{d}t+\int_{T_1}^{T_2}A(t)A(t+\tau)\mathrm{d}t\right] = E[A(t)A(t+\tau)]. \tag{2}$$

The distance between two observation points is fixed as $l_x\sim u\tau_e$ and $l_y\sim v\tau_e$. Let $A(j)$ and $A(m)$ be in the same turbulent field, and they have the same sampling frequency and time interval Δt. The more each series conforms to the ergodicity of the turbulent field, the more their mean value μ_A and autocorrelation function $R_A(\tau)$ tend to be consistent. If τ_e=0, the period difference between the first and second halves of the new series can be eliminated. This is equivalent to taking two pieces of a very long series and splicing them together without changing the relaxation time of the random process. The smooth randomness of the original turbulence is preserved. At the same time, as long as the interception period is long enough, the statistical requirements can be guaranteed. Based on the above relationship, the conditions for judging the ergodicity of the turbulence mean value and autocorrelation function are as follows:

$$Ero(A) = \lim_{T\to\infty}\frac{1}{T}\int_0^{2T}\left(1-\frac{\tau}{2T}\right)\cdot\left[R_A(\tau)-\mu_A^2\right]\mathrm{d}\tau = 0, \tag{3}$$

$$Er(A) = \lim_{T\to\infty}\frac{1}{T}\int_0^{2T}\left(1-\frac{\tau'}{2T}\right)\left[B(\tau') - \left|R_A(\tau)\right|^2\right]\mathrm{d}\tau' = 0, \tag{4a}$$

$$B(\tau') = E\{A(t+\tau+\tau')A(t+\tau')[A(t+\tau)A(t)]\}. \tag{4b}$$

If the combination of the data observed at the two sites satisfies the ergodicity, the turbulence spectrum can be determined by performing the following Fourier transform on the new time-series combination.

$$F_A(n) = \frac{1}{2N}\left[\sum_{j=0}^{N-1}A(j)\cos\left(\frac{2\pi nj}{N}\right)+\sum_{m=N}^{2N-1}A(m)\cos\left(\frac{2\pi nm}{N}\right)\right] - \frac{i}{2N}\left[\sum_{j=0}^{N-1}A(j)\sin\left(\frac{2\pi nj}{N}\right)+\sum_{m=N}^{2N-1}A(m)\sin\left(\frac{2\pi nm}{N}\right)\right]. \tag{5}$$

Even if the sampling period of two sets of data is the same, the period τ_e will be artificially introduced, and the maximum energy spectrum error will affect the eddy of the τ_e scale and the nearest $n\tau_e$ scale. The artificial influence on $F_A(n)$ can be eliminated only when τ_e=0. This condition is consistent with the requirements of a stationary random process. The frequency range of the surface-layer turbulence observation is 10^1–10^{-4} Hz, and a sampling frequency of 10 Hz in an actual observation can precisely control the period τ_e within a few seconds ($\tau_e\to0$). Under normal conditions, the period scale of several seconds corresponds to the inertial sub-range of turbulence, and the turbulence energy is 1–2 orders of magnitude smaller than the energy in the containing-energy range, so the energy spectrum error can be ignored. Moreover, the turbulence spectrum determined at two sites will introduce a spurious energy spectrum in the low-frequency part n<2. At the same time, due to the folding property of the Fourier transform, the error will occur when the highest frequency part n>N/4. Similarly, the above process can be extended to the analysis of the turbulent energy spectrum of multi-site observations; that is, each site is projected onto the mean streamline and τ_e is determined using l_x~$u\tau_e$. Then, when concatenating the time series of velocity variables, the data of each site sequentially delay τ_e based on the order of upstream and downstream, so $\tau_e\to0$ between each series.

2.2 Turbulence spectrum and turbulence structure function

The turbulence spectrum of the atmospheric boundary layer for three scales can respectively be written as (Stull, 1988):

$$kS_u(k) = C_1\varepsilon^{2/3}k^{-2/3}, 1/z < k < 1/\eta, \tag{6}$$

$$kS_u(k) = C_2k^0, 1/\delta < k < 1/z, \tag{7}$$

$$kS_u(k) = C_3k^1, k < 1/\delta, \tag{8}$$

where the lower corner subscripts u represents the horizontal and longitudinal wind velocity; C_1, C_2, and C_3 are undetermined coefficients; and ε is the dissipation rate of the turbulent kinetic energy. The turbulence second-order structure function is $D_{uu}(r) = \overline{\left[A(x+r\hat{e}_x)-A(x)\right]^2}$. Corresponding to the turbulence spectrum, the second-order structure functions of eddies at different scales are satisfied (Kolmogorov, 1941, 1962; Lindborg, 1999; Ghannam et al., 2018):

$$D_{uu}(r) = C\varepsilon^{2/3}r^{2/3}, \eta < r < l, \tag{9}$$

$$D_{uu}(r) = B + A\ln\left(\frac{r}{l}\right), l < r < \delta, \tag{10}$$

$$D_{uu}(r) = 2\left[B_1 - A_1\ln\left(\frac{z}{\delta}\right)\right], r \sim \delta, \tag{11}$$

where, C, A, and B are corresponding constants. The characteristic scale l is the critical scale to distinguish between isotropic and non-isotropic turbulence, so it has the same magnitude as the observed height, l~z. The horizontal cross velocity and vertical velocity have similar characteristics of the second-order structure function. The wavelength k and wavenumber λ satisfy the relation k=1/λ, and r is essentially regarded as a series of wavelengths. Obviously, the turbulence second-order structure function should correspond to the turbulence spectrum (Ghannam et al., 2018). Therefore, the time series established by the multi-site observation can estimate the turbulence spectrum accurately, and the turbulence second-order structure function can be estimated accurately and be consistent.

Usually, the second-order structure function is determined by a single-site turbulence observation under the ergodicity condition, which is denoted as D_{ut} or D_{vt} in this paper. In theory, the second-order structure function is the statistical average of the squared difference between u or v in the downstream and u or v in the upstream of the flow field. They describe the spatial statistical characteristics of eddies at different scales, which are denoted as D_{ur} or D_{vr}. D_{ut}=D_{ur} and D_v =D_{vr} can be satisfied only when the turbulence observation satisfies the ergodicity. Therefore, compared to the relation of the M–O similarity (Chen et al., 2015), a comparison of the second-order structure function determined by a single-site observation with the second-order structure function determined by a two-site observation is a more reasonable scheme to verify the ergodicity of turbulence observations.

3. Site and data preprocessing

Pingliang Land Surface Process and Severe Weather Research Station, CAS (35°34′36.70″N, 106°42′09.02″E; altitude of 1603 m; Pingliang Station for short) is located in

Baimiao, Pingliang, Gansu (Figure 1a), which is a typical tableland terrain. The topographic features and instruments are described in detail in the literature (Chen et al., 2021). The position and wind direction of the six eddy-covariance systems concerned in this paper are shown in Figure 1. A tow represents a 20 m tower erected in the middle of the field, with two eddy-covariance systems at 7.25 and 14.20 m (including a 3D ultrasonic wind and temperature instrument CSAT3 and an infrared gas analyzer Li7500). sn1–sn4 are four sets of CSAT3 with a height of 5.10 m. The distance and direction between them are indicated in Figure 1. Each of the four CSAT3 sets is located in a cornfield, and their sampling frequency was all at 10 Hz. Before the experiment, four sets of CSAT3 and 7.25 m CSAT3 were tested with a zero drift velocity. The experiment started from March 2017 to September 2017. During this period, the main crops in the farmland were corn, winter wheat, and flax, and some farmlands were planted with pine saplings, elm saplings, alfalfa, and other cash crops. During the experiment period, the plant height from 6/16 to 6/24 was relatively uniform, and the vegetation height of different farmlands in the other periods greatly varied (for more details, see the literature (Chen et al., 2021)). Before the data analysis, error data due to circuit pulse and other reasons in the observed data were deleted. The ultrasonic temperature pulsation was modified to absolute-temperature pulsation (Schotanus et al., 1983; Kaimal and Gaynor, 1991). Before and after the experiment, the inclination of each instrument was corrected by a full-temperature biaxial digital inclination sensor (RION). Data preprocessing was consistent with the processing method in another thesis (Chen et al., 2021).

In addition, before the data analysis, the period duration τ_e between the upstream and downstream was first determined based on the average velocity of each 1 h data. After the artificial period was eliminated by sequentially delaying the initial time, 36000×4 sample values were obtained by connecting the data of four sites head to tail. In this method, 2106 sets of 1 h data were obtained. Then, new datasets were used to test the ergodicity of the turbulence observation, and the turbulence spectrum and second-order structure function were further determined. When the second-order structure function was used to verify the ergodicity of the turbulence observation, the data at the two observation sites located downstream of the mean flow field were selected first. Considering the large error of the wind direction observation, when the downstream observation site is within the range of the average wind direction of the upstream observation point (−15°, +15°), the two observation sites are in the upstream and downstream positions of the streamline. Then, the second-order structure function determined by the two observation sites was compared and analyzed with the second-order structure function determined by any observation site upstream and downstream. In addition, the new time series determined from the data of the four observation sites arti-

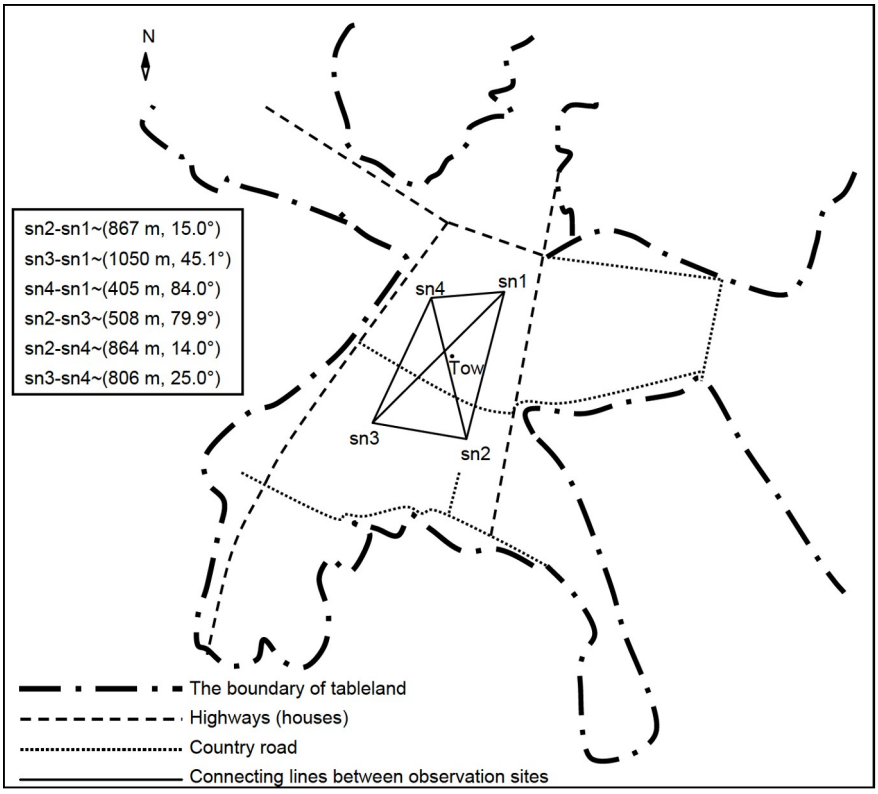

Figure 1 Topographic map of the observation area and position of four sets of eddy correlation systems.

ficially increased the total turbulence energy, so the energy density spectrum was used in the analysis of the turbulence spectrum. The M–O stratification stability $(z-d)/L=-\kappa g(z-d)\overline{w'\theta'}_v/\left(u_*^3\overline{\theta}_v\right)$ was directly determined using the 1 h observation data, and the displacement height d was taken as 1/3 of the maize height (Stull, 1988; Chen et al., 2021).

4. Results

4.1 Ergodicity of the turbulence observation

Single-site turbulence observations have shown that under unstable stratification conditions, the observation of large-scale eddies larger than 10 min cannot easily meet the ergodicity requirement (Chen et al., 2021). For the sake of illustration, the selected data were from 11:30 to 12:30 on August 31, 2017, whose stability parameter $(z-d)/L$=−5.79 were determined through a single-site observation with an average wind speed of 0.76 m s^{-1}. Their ergodicity functions with varying τ are shown in Figures 2 and 3. For comparison, Figure 2a and 2b is the average ergodicity function, and $Ero(A)/\sigma_A^2$ (σ_A^2 is the turbulence variance of the variable), normalized by the temperature and velocity turbulence variance derived from 40 min and 60 min high-pass filtering data at the four sites. Figure 2c shows that $Ero(A)/\sigma_A^2$ after 40 min high-pass filtering at a single-site observation varies with τ (Chen et al., 2021). The amplitude of $Ero(A)/\sigma_A^2$ of the velocity and temperature with a scale below 40 min from the four-site observation was more convergent to 0 than that from the single-site observation. Even when compared with $Ero(A)/\sigma_A^2$ obtained from the single-site observation for 40 min high-pass filtering, the amplitude of $Ero(A)/\sigma_A^2$ with a scale below 60 min from the multi-site observation decreased and converged to 0, which can easily meet the ergodicity of the turbulence observation. At the same time, although the amplitude of $Ero(\theta)/\sigma_\theta^2$ of temperature becomes large due to the difference in temperature at each observation site, the convergence trend of $Ero(\theta)/\sigma_\theta^2$ is still good. Corresponding to Figure 2, Figure 3 shows the variation of the normalized autocorrelation function $Er(A)/\sigma_A^4$ as a function of the relaxation time τ. The part with τ coordinates less than 1 min is the logarithmic coordinate, whereas the part with τ coordinates greater than 1 min is the linear coordinate. Figure 3a and 3b is the results after the 40 min and 60 min high-pass filtering from the four-site observation, respectively, and Figure 3c is the results after the 40 min high-pass filtering from the single-site observation. After 40 min high-pass filtering, the convergence of $Er(A)/\sigma_A^4$ from the four-site observation was compared with that of $Er(A)/\sigma_A^4$ from the single-site observation. The normalized autocorrelation function of the longitudinal velocity, vertical velocity, and temperature started to converge after τ>0.3 min, and its

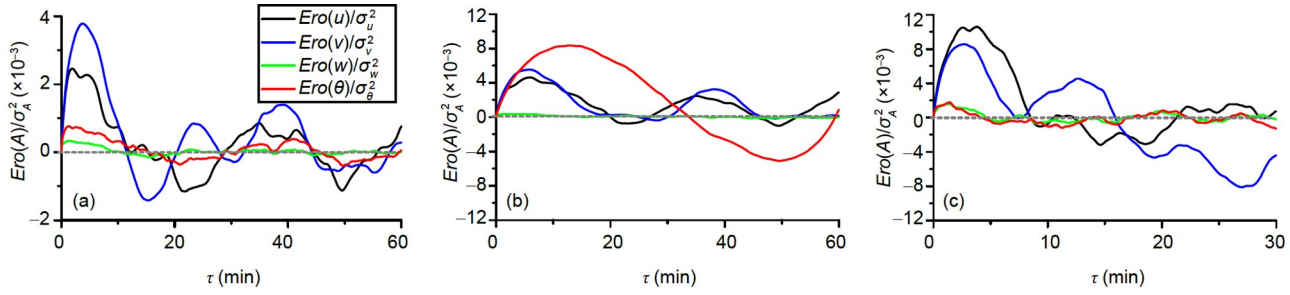

Figure 2 Comparison of the ergodicities of the 1 h wind velocity and temperature turbulence mean values derived from the four-site and single-site observation. Under extremely unstable stratification, (a) and (b) are the normalized functions vs τ after 40 min and 60 min high-pass filtering from the four-site observation, and (c) that after 40 min high-pass filtering from the single-site observation.

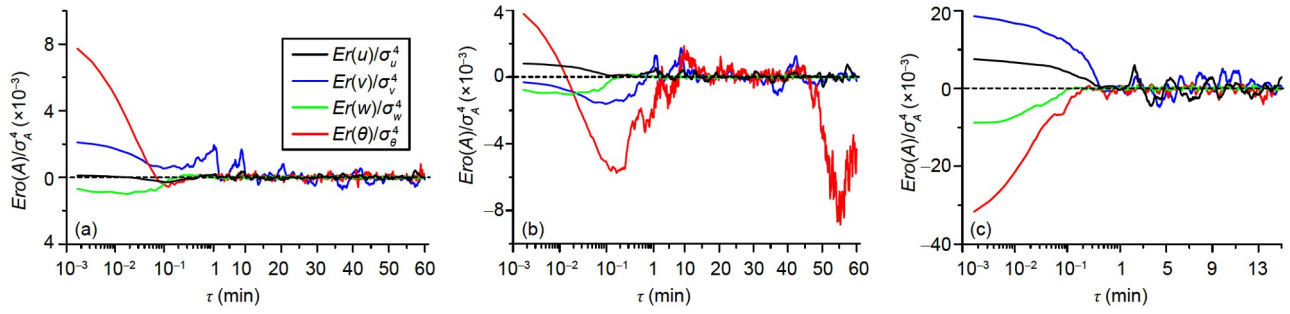

Figure 3 Comparison of the ergodicities of the 1 h wind velocity and temperature autocorrelation functions derived from the four-site and single-site observation. Under extremely unstable stratification, (a) and (b) are the normalized autocorrelation functions after 40 min and 60 min high-pass filtering from the four-site observation, and (c) that after 40 min high-pass filtering from single-site observation.

amplitude was one order of magnitude smaller. However, $Er(v)/\sigma_v^4$ of the cross velocity started to converge after $\tau>$ 2 min, and its amplitude was also about one order of magnitude smaller than that of the single-site observation. For the convergence of $Er(A)/\sigma_A^4$ after the 60-min high-pass filtering from the four-site observation, the amplitude of $Er(A)/\sigma_A^4$ for the longitudinal velocity and vertical velocity was slightly larger than that after the 40 min high-pass filtering, but it was also about one order of magnitude smaller than that from the single-site observation. However, $Er(A)/\sigma_A^4$ of the cross velocity and temperature did not converge until $\tau>5$ min. In particular, the $Er(\theta)/\sigma_\theta^4$ convergence of the temperature was broken for 45 min$<\tau$. These results imply that, for four-site observations, eddies less than the scale of 60 min can easily satisfy ergodicity. However, the thermal difference of the complex surface will make the effect of the temperature difference of 60-min scale eddies on $Ero(\theta)/\sigma_\theta^2$ and $Er(\theta)/\sigma_\theta^4$ prominent. At the same time, the convergence of the longitudinal velocity and temperature autocorrelation function with relaxation time was obviously worse in the first 5 min, so eddies smaller than the 5 min scale are local at each site. Excluding the initial stage of extreme weather processes, such as thunderstorms, from the unstable, neutral, to weakly unstable stratification, eddies less than the 60 min scale observed by the four sites easily met ergodicity (figure omitted).

4.2 Second-order structure function of the turbulence and verification of the ergodicity

Based on the positions of the four observation sites, the turbulent field can pass through the four observation sites within 1 h only when the average wind speed $u>0.4$ m s^{-1}. Moreover, when the wind speed is high, the large-scale eddy energy spectrum can easily meet $kS_u \sim k^{+1}$. Figure 4 shows the second-order structure functions of the turbulent longitudinal and cross velocity when the average wind speed is 2.47 m s^{-1} (wind direction is 224°) from 12:00 to 13:00 on a sunny day on May 27. During this period, the average cross velocity in 1 min reached 2.04 m s^{-1}, and the turbulence field in 1 h could pass four sites in the longitudinal and cross directions. At the same period, the height difference of the vegetation was relatively small. To clearly display various scales of eddies, the results of the attached eddies and large-scale eddies with $r>100$ m are also displayed in linear coordinates in addition to logarithmic coordinates as a whole. The results show that there are some differences in the structure functions at the four sites, but the results of each site show that the scale of the attached eddy is approximately 500 m$>r>$100 m, whereas the scale of the large-scale eddy is approximately $r>500$ m. In particular, for the second-order structure function of the large-scale eddy of the horizontal velocity, the fluctuation at different sites can be more than two times. Therefore, we can compare the turbulent second-order structure function determined by a single-site observation to that determined by the two-site observation to verify the ergodicity of each single-site observation.

To verify the ergodicity of the turbulence observation using the second-order structure function of the horizontal velocity, all data were first filtered for 10 min, 20 min, and 40 min high-pass and were grouped for 1 h. Finally, 1524 groups of preprocessed data were obtained. Figure 5 shows the variation of the velocity second-order function D_{ut} of the single-site observation and the velocity second-order function D_{ur} of the two-site observation with time after 60 min filtering. Their fluctuation is consistent. Then, the consistency of the filtered and unfiltered results at different scales was compared using the linear fitting $D_{ut}=D_{ur}$. The results in Figure 6 show that from 10 min to 20 min and then to 40 min, the linear fitting results between the two second-order functions gradually become worse. The linear fitting result of $D_{ut}=D_{ur}$ after 60 min filtering is the worst. The results indicate that, with the increase in time and space scale, the ergodicity of the turbulence observation at a single site becomes worse. The larger the time and space scale, the more

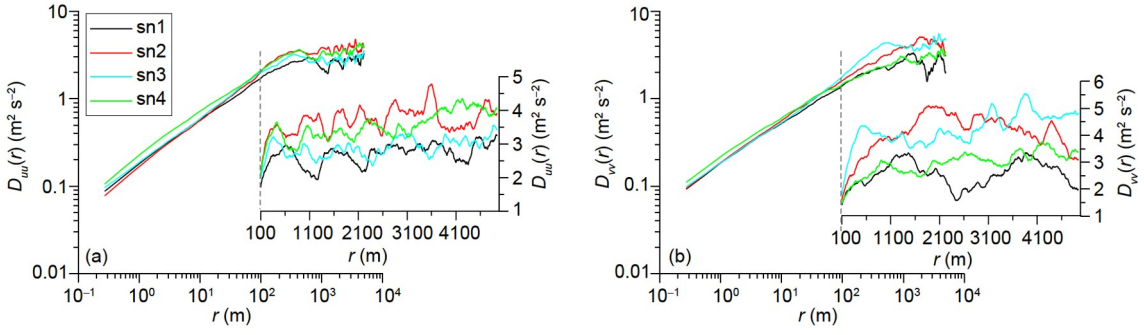

Figure 4 Second-order structure functions of the longitudinal and cross velocities. (a) and (b) are the second-order structure function of the longitudinal and cross winds with an average wind velocity of 2.47 m s^{-1} (wind direction of 224°) from 12:00 to 13:00 on May 27, respectively. To show the details of the second-order structure functions of the large-scale eddies and attached vortices, the linear coordinates are used for $r>100$ m in the additional diagram.

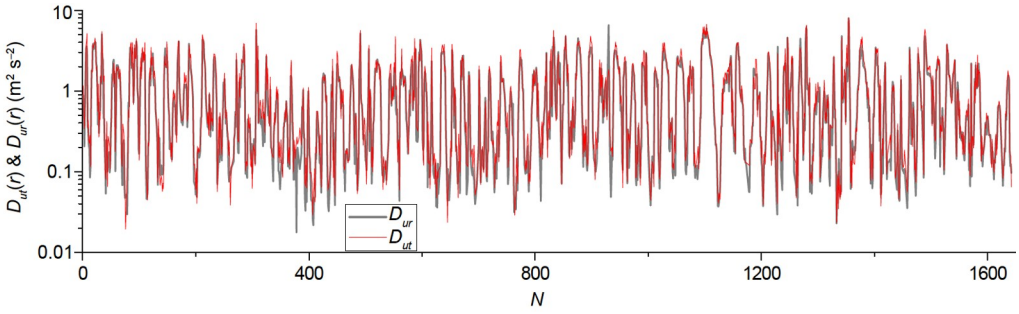

Figure 5 Variable of the second-order structure function of the longitudinal velocity determined by the single-site and two-site data with time after 60 min high-pass filtering.

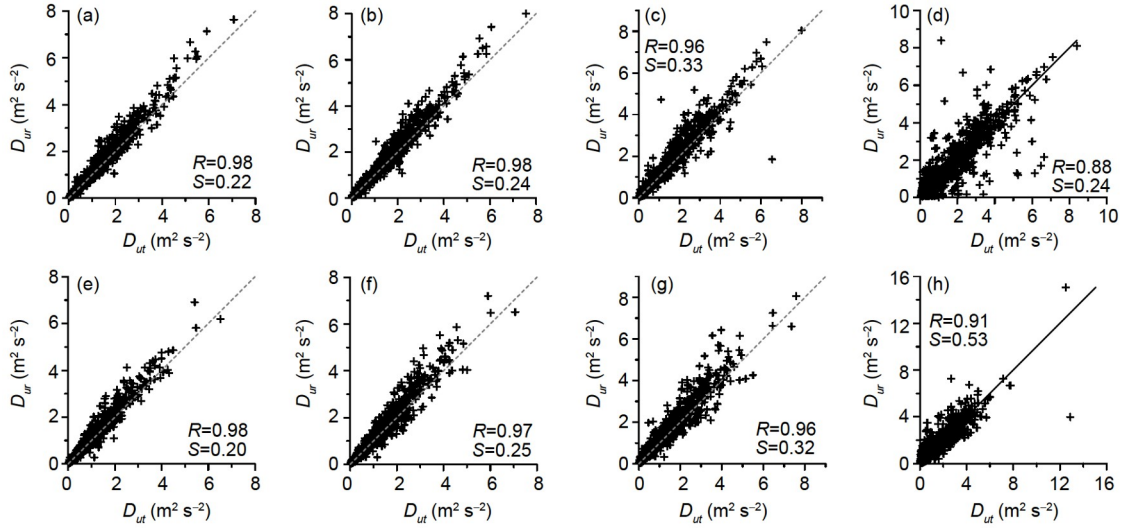

Figure 6 Fitting linear relationship (D_{ut}=D_{ur}) between the second-order structure functions of the turbulent velocity determined by single site and two sites for the eddies with different scales. (a)–(d) are the fitting linear relationships, D_{ut}=D_{ur}, related to the longitudinal velocity after 10 min, 20 min, and 40 min high-pass filtering and without filtering, respectively; (e)–(h) are the fitting linear relationships, D_{vt} = D_{vr}, related to the cross velocity after 10 min, 20 min, and 40 min high-pass filtering and without filtering, respectively.

difficult the turbulence observation is to meet ergodicity. This condition also validates the ergodicity result determined by the functional relations $Ero(A)/\sigma_A^2$ and $Er(A)/\sigma_A^4$. At the same time, the results in Figure 6 indirectly reflect the accuracy of the eddy kinetic energy with different scales, which are observed by a single-site observation.

Figure 7 shows the longitudinal and cross second-order structure functions of the wind velocity determined from the data of the four sites, which is the same as the diagram in Figure 4. The logarithmic coordinate was used for the overall demonstration, and the results of the attached eddies and large-scale eddies with r>100 m are displayed in linear coordinates. The results show that the second-order structure function D_{uu}=D_{vv} ~ $r^{2/3}$, spatial scale r<200 m, and corresponding time scale t <81 s. For the observed height z, the spatial scale of the attached eddies (D_{uu}~ln(r/z), D_{vv}~ln(r/z)) is approximately 200–600 m, and the corresponding time scale is approximately 81–243 s. Due to the dynamic shear of the surface, D_{uu} of the maximum eddy (r≈600 m) of the longitudinal velocity suddenly decreased. The spatial scale of large-scale eddies is approximately r>600 m, and the corresponding time scale is t>243 s. Moreover, the second-order structure function of the velocity of large-scale eddies is closer to a constant, i.e., D_{uu}≈C, D_{vv}≈C.

4.3 Estimating the turbulence spectrum from the four-site observation

In Figure 8, the turbulence spectra determined by the four-site and single-site data are compared using the turbulent energy spectral density. There are significant differences between them, especially the energy spectra of large-scale eddies, which are of the order of 1–2. Moreover, the spectrum segments corresponding to the large-scale eddies (S_u~f^0), attached eddy (S_u~f^{-1}), and separated eddy (S_u~$f^{-5/3}$) determined by the four-site data were significant, which were f<1.81×10^{-3} Hz (552 s), 1.81×10^{-3} Hz<f<9.17×10^{-3}, and 9.17×10^{-3} Hz<f, respectively. Three temporal scales esti-

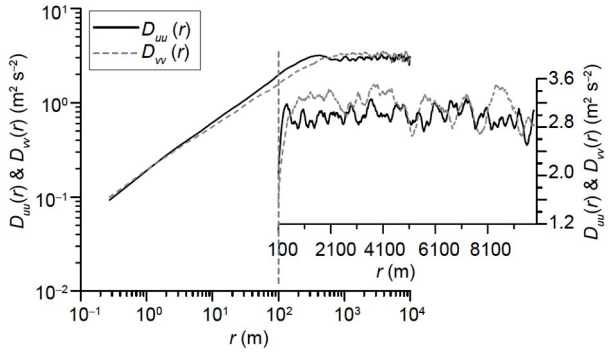

Figure 7 Second-order structure functions of the longitudinal (black solid line) and cross (gray dotted line) velocities estimated from the four-site observation. The coordinate of r are the same as that in Figure 4.

mated by the four-site data are in good agreement with those determined by the second-order structure function. In addition, as the boundary between the mesoscale weather system and small-scale boundary-layer system (Larsen et al., 2016), the wind velocity spectral gap is very clear in the turbulence spectrum determined at the four sites, and they consistently correspond to the range of approximately 4.2×10^{-4}–6.9×10^{-4} Hz (20–40 min scale). However, the temperature spectrum has no clear gap, and this feature is consistent with the turbulence spectrum determined at a single site for 6 h (Chen et al., 2021). If only the velocity spectrum determined by 1 h data of a single site is used as a reference, the spectral gap scale may be determined in the range of a few minutes. At the same time, the temperature turbulence spectrum determined at a single site also has an obvious deviation. The large-scale eddy spectrum determined by the four sites is accurate in combination with the ergodicity of the four-site observation. Certainly, the importance of a single-site observation cannot be completely denied because it can describe the turbulent structure of the vertical section along the flow field. For example, on the vertical section flowing through sn1, sn3, and sn4, for the cross and vertical wind velocity turbulence, the intensity of the eddy at the scale of approximately 8 minutes is small, whereas the intensity of the cross and vertical wind velocity turbulence at the same scale flowing through sn2 is still large. In combination with the single-site longitudinal wind velocity and temperature spectrum and multi-site longitudinal wind velocity and temperature turbulence spectrum, the eddy at this scale has a flat longitudinal narrow structure.

4.4 Covariance between the vertical velocity and temperature determined by the four-site observation

The observed turbulence by the four-site observation can satisfy ergodicity and is comprehensive, and the accuracy of the turbulent flux is high. Figure 9 shows the Ogive functions for the vertical velocity and temperature covariance determined by the four-site and single-site observations, respectively. The results show that the Ogive functions of $\overline{w'\theta'}_v$ determined by each site are obviously different due to the poor uniformity and the thermodynamic and kinetic difference of the underlying surface. The Ogive function of $\overline{w'\theta'}_v$

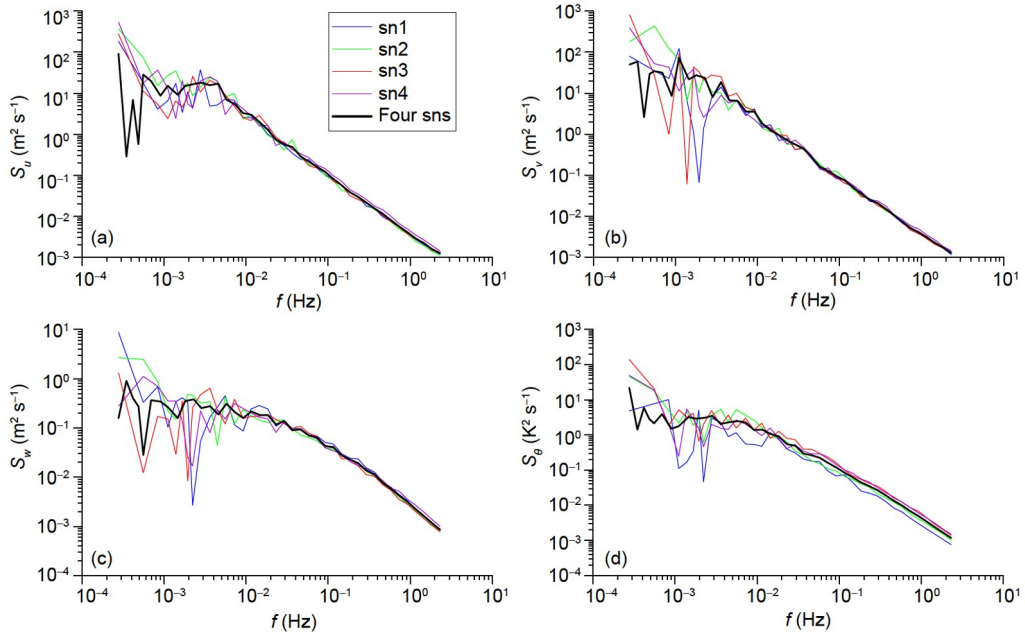

Figure 8 Turbulence spectra estimated from single-site and four-site observations. (a)–(d) are longitudinal, cross and vertical wind velocities, and temperature turbulence spectra from 12:00 to 13:00 on May 27, respectively. The blue thin line is the turbulence spectrum of the sn1 site, the green thin line is the turbulence spectrum of the sn2 site, the red thin line is the turbulence spectrum of the sn3 site, the purple thin line is the turbulence spectrum of the sn4 site, and the black thick line is the turbulence spectrum determined by the four-site observation.

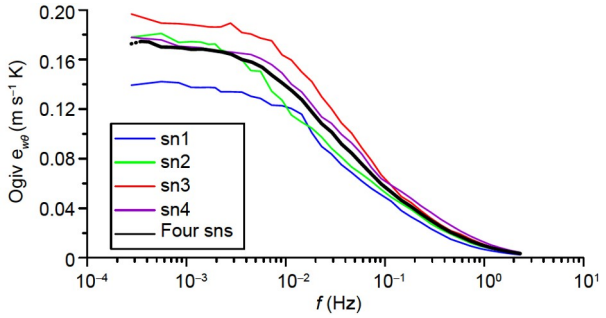

Figure 9 Ogive functions of the vertical velocity and temperature covariance estimated from the single-site and four-site observations.

jointly determined by the four-site observation is in the middle of the Ogive functions for the vertical velocity and temperature covariance of each site.

5. Discussion

The ensemble average theory of turbulence proposes that the ergodicity of the turbulence observation can be improved by adding turbulence observation points. The experimental analysis proves this conclusion. Essentially, the scales and intensities of detached eddies determined by the velocity spectrum and the velocity second-order structure function are different on each streamline of the turbulent field in the single-site observation. With the increase in scale, the velocity spectrum and velocity second-order structure function on each streamline significantly vary. The eddies of 10^0–6×10^2 s scale can easily meet the ergodicity in the single-site observation (Chen et al., 2015), but large-scale eddies usually cannot satisfy the ergodicity with their scale ranging from 10^2 to 10^4 s with non-isotropic complex structures. The large-scale eddy on the streamline described by each site is only a segment of the eddy, so the turbulence spectrum and second-order structure function determined by the single-site observation are fragmentary. More comprehensive turbulence field information can only be obtained using reasonably arranged multi-site observation. Similarly, although large-scale eddies may be deformed due to their proximity to the surface, the spectra of detached eddies, attached eddies, and large-scale eddies determined by the four-site observation are clear. The results of the four-site observation are the regional ensemble average for smaller-scale eddies when large-scale eddies are determined comprehensively. Kolmogorov (1941) pointed out that the velocity second-order structure function is the result of the streamline. The feature of the large-scale eddy spectra determined by the four-site observations indicates that the turbulent large-scale eddies obtain energy, and then the energy is transferred to the next-scale eddy by the energy cascade. Although there are differences in the energies of the next-scale eddies along various streamlines, and the energies can either increase or decrease due to the topographic influence, the total energy is under the constraint of the energy cascade. In summary, the scale range of eddies in the surface layer is from 10^{-1} to 10^4 s (10^{-5}–10^2 km), which is from isotropic eddies to non-isotropic eddies and the turbulence spectrum gap. To comprehensively and carefully observe the turbulence field, combining single-site and multi-site observations is obviously necessary for the experimental analysis. Moreover, in the multi-site observation, the distribution of each site should be based on the ergodicity of the single-site turbulence observation, and the scale range of the large-scale eddies in the surface layer should be considered. The number of observation sites and spatial layout should be determined based on the comprehensive grasp of the turbulence structure in the observation area. Based on the experimental observation results of the turbulent system with a large-scale span and extreme complexity, the ergodicity of the multi-site observation also provides a research clue for the scale transformation problem in similar fields.

In the surface layer, the turbulent flux is the result of full-scale eddy transport. Therefore, the vertical flux of the turbulence is essentially the amount of energy and matter transported by eddies in the flow field that has the same size as the eddy scales. The accuracy of the turbulent flux determined by the multi-site observation is always higher than that determined by the single-site observation. As long as the eddies at various scales in the turbulence observation meet the ergodicity, the accuracy of the turbulence observation can be guaranteed, regardless of how complex the turbulence field and its environmental conditions are. In this way, the M–O similarity relation obtained under horizontal uniformity and steady-state conditions can no longer be used to ensure the quality of the turbulence observation under complex conditions (Foken et al., 2004).

6. Conclusions

In the complicated condition of the Loess Plateau, with the complex turbulent structure and wide range eddy scale, the requirements of the Reynolds mean theory can be easily met using four-site observations in the eddy-covariance method, so the observation accuracy of large-scale eddies can be improved.

(1) The comparison results of the velocity turbulence second-order structure functions determined by a single point and two points are reasonable to verify the ergodicity of the turbulence observation.

(2) The four-site turbulence observation allows the eddy within the scale of 60 min to easily meet the ergodicity, which can ensure the comprehensiveness of the turbulence observation and improve the estimation accuracy of the

turbulence spectrum and flux.

(3) After eliminating the artificial period error between multi-site observation data, the turbulence spectrum and second-order structure function of the wind velocity can accurately describe the energy spectrum characteristics and corresponding scales of attached and large-scale eddies consistently and clearly. At the same time, the spatial and temporal scales of the spectral gap in the tableland were approximately 20–40 min and 3–6 km, respectively.

Thus far, this study has established a turbulence observation scheme under complex conditions, which is based on the Reynolds mean theory and does not need to satisfy the assumptions of steadiness and horizontal uniformity.

Acknowledgements *Special thanks to the Pingliang Land Surface Process and Severe Weather Research Station for providing strong support for the field experiments. This work was supported by the National Natural Science Foundation of China (Grant Nos. 42175104 & 41675014).*

References

Biferale L, Procaccia I. 2005. Anisotropy in turbulent flows and in turbulent transport. Phys Rep, 414: 43–164

Chen J, Hu Y, Yu Y, Lü S. 2015. Ergodicity test of the eddy-covariance technique. Atmos Chem Phys, 15: 9929–9944

Chen J, Chen X, Jing X, Jia W, Yu Y, Zhao S. 2021. Ergodicity of turbulence measurements upon complex terrain in Loess Plateau. Sci China Earth Sci, 64: 37–51

Drobinski P, Carlotti P, Newsom R K, Banta R M, Foster R C, Redelsperger J L. 2004. The structure of the near-neutral atmospheric surface layer. J Atmos Sci, 61: 699–714

Foken T, Goockede M, Mauder M, Mahrt L, Amiro B, Munger W. 2004: Post-Field Data Quality Control. 181–208. In: Lee X, Massman W J, Law B. 2004. Handbook of Micrometeorology: A Guide for Surface Flux Measurement and Analysis. New York: Atmospheric and Oceanographic Sciences Library, Kluwer Academic Publishers, 250

Ghannam K, Katul G G, Bou-Zeid E, Gerken T, Chamecki M. 2018. Scaling and similarity of the anisotropic coherent eddies in near-surface atmospheric turbulence. J Atmos Sci, 75: 943–964

Hu Y Q, Chen J B, Zuo H C. 2007. Theorem of turbulent intensity and macroscopic mechanism of the turbulence development. Sci China Ser D-Earth Sci, 50: 789–800

Hunt J C R, Carlotti P. 2001. Statistical structure at the wall of the high Reynolds number turbulent boundary layer. Flow turbulence combust, 66: 453–475

Kaimal J C, Gaynor J E. 1991. Another look at sonic thermometry. Bound-Layer Meteorol, 56: 401–410

Kolmogorov A N. 1941. Local structure of turbulence in an incompressible viscous fluid at very high Reynolds numbers. Sov Phys Usp, 10: 734–746

Kolmogorov A N. 1962. A refinement of previous hypotheses concerning the local structure of turbulence in a viscous incompressible fluid at high Reynolds number. J Fluid Mech, 13: 82–85

Larsén X G, Larsen S E, Petersen E L. 2016. Full-scale spectrum of boundary-layer winds. Bound Layer Meteor, 159: 349–371

Lindborg E. 1999. Can the atmospheric kinetic energy spectrum be explained by two-dimensional turbulence? J Fluid Mech, 388: 259–288

Liu S, Xu Z, Song L, Zhao Q, Ge Y, Xu T, Ma Y, Zhu Z, Jia Z, Zhang F. 2016. Upscaling evapotranspiration measurements from multi-site to the satellite pixel scale over heterogeneous land surfaces. Agric For Meteor, 230-231: 97–113

Oncley S P, Friehe C A, Larue J C, Businger J A, Itsweire E C, Chang S S. 1996. Surface-layer fluxes, profiles, and turbulence measurements over uniform terrain under near-neutral conditions. J Atmos Sci, 53: 1029–1044

Oncley S P, Foken Th, Vogt R, Bernhofer Ch, Kohsiek W, Liu H, Pitacco A, Grantz D, Ribeiro L, Weidinger T. 2002. The energy balance experiment EBEX-2000. Proceedings 15th symposium on boundary layers and turbulence 15–19 July (2002), Wageningen, The Netherlands

Pavidson D A. 2004. Turbulence an Introduction for Scientists and Engineers. Oxford University Press Inc, New York, 657

Poulos G S, Blumen W, Fritts D C, Lundquist J K, Sun J, Burns S P, Nappo C, Banta R, Newsom R, Cuxart J, Ter-radellas E, Balsley B. 2002. CASES-99: A comprehensive in-vestigation of the stable nocturnal boundary layer. Bull Amer Meteor Soc, 83: 55–581

Richardson L F. 1922. Weather Prediction by Numerical Process. London: Cambridge University Press, 236

Schotanus P, Nieuwstadt F T M, de Bruin H A R. 1983. Temperature measurement with a sonic anemometer and its application to heat and moisture fluxes. Bound-Layer Meteorol, 26: 81–93

Stull R B. 1988. An Introduction to Boundary Layer Meteorology. Dordrecht: Atmospheric Sciences Library, Kluwer Academic Publishers. 670

Taylor G I. 1935a. Statistical theory of turbulence I. Proc Royal Society A: 421–444

Taylor G I. 1935b. Statistical theory of turbulence II. Proc Royal Society A: 444–454

Taylor G I. 1935c. Statistical theory of turbulence III. Proc Royal Society A: 455–464

Taylor G I. 1935d. Statistical theory of turbulence IV. Proc Royal Society A: 465–478

Zhang Q, Li H Y, Zhao J H. 2012. Modification of the land surface energy balance relationship by introducing vertical sensible heat advection and soil heat storage over the Loess Plateau. Sci China Earth Sci, 55: 580–589

Zuo H C, Xiao X, Yang Q D, Dong L X, Chen J W, Wang S J. 2012. On the atmospheric movement and the imbalance of observed and calculated energy in the surface layer. Sci China Earth Sci, 55: 1518–1532

(Responsible editor: Jianping HUANG)